Organic long-persistent-luminescence stimulated by visible light in p-type systems based on organic photoredox catalyst dopants

Kazuya Jinnai[1,2], Ryota Kabe[2,3]*, Zesen Lin[2,3], and Chihaya Adachi[1,2,4]*

[1] Center for Organic Photonics and Electronics Research (OPERA), Kyushu University, 744 Motooka, Nishi-ku, Fukuoka 819-0395, Japan

[2] JST, ERATO Adachi Molecular Exciton Engineering Project, 744 Motooka, Nishi-ku, Fukuoka 819-0395, Japan

[3] Organic Optoelectronics Unit, Okinawa Institute of Science and Technology Graduate University, 1919-1 Tancha, Onna-son, Kunigami-gun, Okinawa 904-0495, Japan

[4] International Institute for Carbon Neutral Energy Research (I^2CNER), Kyushu University, 744 Motooka, Nishi-ku, Fukuoka 819-0395, Japan

Abstract

Organic long-persistent-luminescent (OLPL) materials demonstrating hour-long photoluminescence have practical advantages in applications owing to their flexible design and easy processability. However, the energy absorbed in these materials is typically stored in an intermediate charge-separated state that is unstable when exposed to oxygen, thus preventing persistent luminescence in air unless oxygen penetration is suppressed through crystallization. Moreover, OLPL materials usually require ultraviolet excitation. Here we overcome such limitations and demonstrate amorphous OLPL systems that can be excited by radiation up to 600 nm and exhibit persistent luminescence in air. By adding cationic photoredox catalysts as electron-accepting dopants in a neutral electron-donor host, stable charge-separated states are generated by hole diffusion in these blends. Furthermore, the addition of hole-trapping molecules extends the photoluminescence lifetime. By using a p-type host less reactive to oxygen and tuning

the donor–acceptor energy gap, our amorphous blends exhibit persistent luminescence stimulated by visible light even in air, expanding the applicability of OLPL materials.

Main

Long-persistent luminescence (LPL) is a phenomenon in which emission continues for a long period after photoexcitation[1]. LPL emitters are used as glow-in-the-dark paints for clock faces and emergency lights. High-efficiency LPL materials are composed of metal-oxide microcrystals and small amounts of rare-earth ions that act as charge-trapping and emission sites[2,3]. In these inorganic LPL materials, holes or electrons generated by the photoexcitation of the metal-oxide crystal are accumulated in dopants that act as charge-trapping sites. Gradual charge recombination followed by thermal detrapping produces hour-long emissions[4,5,6]. Inorganic LPL materials are insoluble in any solvent, and require grinding into microparticles before dispersion into solvents or polymers for practical applications. Most inorganic LPL systems require ultraviolet to blue excitation light below 450 nm due to the limited metal-oxide absorption bands[7,8,9].

We have reported LPL emissions from mixtures of organic molecules[10]. This organic LPL (OLPL) system can be fabricated from a solution process[11] and the fabricated films can be transparent and flexible[12]. LPL emissions can be tuned from greenish-blue to red with the addition of fluorescent materials[13]. In contrast to conventional organic room-temperature phosphorescent (RTP) materials[14], which store their energy in triplet excited states and exhibit radiative transition from the triplet excited states to the singlet ground states[15], OLPL systems accumulate energy into charge-separated states similar to inorganic LPL materials. LPL and RTP can be identified from their emission decay profiles[16,17,18].

Current OLPL systems require inert gas conditions to exhibit LPL because LPL is

quenched completely in air. These OLPL systems, which consist of an electron-donating and electron-accepting material, store absorbed energy into geminate pairs of air-unstable donor radical cations and acceptor radical anions. A donor–acceptor mixed crystal has been reported to exhibit OLPL in air due to oxygen diffusion being suppressed by crystallization[19], but crystalline systems cannot take advantage of OLPL material properties, such as flexibility and processability. Air-stable amorphous OLPL systems will enable applications that are unique to organic materials, such as solution process coating and flexible polymer films. For practical applications of OLPL systems, the air stability needs to be improved without crystallization.

Organic field-effect transistors use radical cations and anions as the active charge-transport species; however, many air-stable organic transistors have been reported[20]. Radical anions (n-type organic semiconductors) are more unstable than radical cations (p-type organic semiconductors) in air. The reported OLPL system can be considered as an n-type OLPL system due to the low donor concentration where only electrons can diffuse through acceptor molecules (Fig. 1a). The unstable radical anions can be ascribed to the high probability of a reaction with oxygen. A p-type OLPL system, in which radical cations diffuse (Fig. 1a), is expected to be more stable to oxygen. Air-stable organic transistors have been achieved by making the lowest unoccupied molecular orbital (LUMO) level deeper than the reduction potential of oxygen (−3.5 eV)[21,22]. To improve the air stability of the OLPL systems, a p-type OLPL system with deep highest occupied molecular orbital (HOMO) and LUMO levels is required.

To satisfy these requirements, we focused on cationic electron acceptors, which are known as a type of organic photoredox catalyst[23]. These organic photoredox catalysts are ideal electron donors or acceptors because of their high reduction or oxidation potential

in the excited state and their ability to form a stable one-electron oxidized or reduced state. Many organic photoredox catalysts have a large enough energy gap to exhibit luminescence in the visible region. Furthermore, a mixture of neutral donors and acceptors forms radical ion pairs ($D^{\delta+}$–$A^{\delta-}$) with Coulombic interaction by photoinduced charge separation, whereas cationic acceptors or anionic donors form neutral radicals rather than radical anions or radical cations ($D^{\delta+}$– $(A^{+})^{\delta-}$, $(D^{-})^{\delta+}$–$A^{\delta-}$) (Fig. 1b). Even if there are counter-ions, the formation of neutral radicals is expected to reduce the Coulombic interaction in the charge-separated state[19,24,25].

Further stabilization of the charge-separated states is required despite the reduced Coulombic interaction. Similar to inorganic LPL systems, the charge-separated state is expected to be stabilized by a special separation of the ion pairs by the introduction of carrier-trapping materials[26,27].

In this article we report p-type OLPL systems made from cationic electron acceptors as a dopant and neutral electron donors as a host. These systems exhibit LPL in air. The addition of hole-trapping materials improved the performance sevenfold under nitrogen gas without changing the emission spectrum. In addition, the p-type OLPL system can be excited by a wavelength from 300 to 600 nm. By tuning the energy gap between the electron donor and acceptor, near-infrared (NIR) LPL emission is achieved. The development of such visible-light-active p-type OLPL systems that work in air will contribute to various future practical applications of OLPL systems.

Cationic photoredox catalysts 2,4,6-triphenylpyrylium tetrafluoroborate (TPP^{+}) and 2,4,6-tris(methoxyphenyl)pyrylium tetrafluoroborate ($MeOTPP^{+}$) were used as electron acceptors[28,29,30] and semiconducting host molecules 3,3′-di(9*H*-carbazol-9-yl)biphenyl (*m*CBP)[31] and 1,3,5-tris(1-phenyl-1*H*-benzimidazol-2-yl)benzene (TPBi)[32] were used as

97 electron donors (Fig. 1c). 4,4′,4″-Tri(9-carbazoyl)triphenylamine (TCTA)[33], 4,4-bis[N-
98 (1-naphthyl)-N-phenylamino]-biphenyl(α-NPD)[34] and 2,8-
99 bis(diphenylphosphoryl)dibenzo[*b*,*d*]thiophene (PPT)[35] were used as hole-trapping
100 materials. The analytical results of these materials by ultraviolet–visible absorption,
101 fluorescence, and phosphorescence spectra are shown in Supplementary Fig. 1. Energy
102 levels of the lowest singlet excited state (^{1}LE) and triplet excited states (^{3}LE) were
103 estimated from the onset of fluorescence and the phosphorescence spectra, respectively.
104 HOMO and LUMO levels were obtained from the first redox peaks of the cyclic
105 voltammograms or differential pulse voltammograms (Supplementary Fig. 2). When the
106 redox potential was out of range of electrochemical measurement, the HOMO and LUMO
107 levels were estimated from the optical gap calculated from the absorption edge (Fig. 1d
108 and Supplementary Table 1).
109 LPL films with a 1:99 molar ratio of an acceptor:donor system were fabricated by
110 conventional melt casting[11]. The obtained films were considered to be amorphous, based
111 on the X-ray diffraction analysis (Supplementary Fig. 3). Steady-state photoluminescence
112 (PL) and LPL spectra, emission decay profiles and steady-state PL quantum yields (Φ_{PL})
113 were obtained under nitrogen gas (Supplementary Fig. 4). Since the emission intensity of
114 LPL is much weaker than that of steady-state PL under photoexcitation, the presented Φ_{PL}
115 do not contain emissions from LPL[36]. The LPL duration was defined as the time until the
116 emission intensity dropped below 1 pW after 300 s of excitation. The triplet charge-
117 transfer excited state (^{3}CT) level was assumed from the singlet charge-transfer excited
118 state (^{1}CT) level that was obtained from the onset of the PL spectrum as most LPL systems
119 have a small energy gap between the ^{1}CT and ^{3}CT (ref. [37]).
120 When the films were excited by 365 nm light, the TPP^+/TPBi, TPP^+/*m*CBP and

MeOTPP$^+$/*m*CBP films exhibited a long LPL emission in which the decay profiles followed a power-law decay (Fig. 2a)[38,39]. Because of the strong electron-accepting properties of TPP$^+$, the mixed film exhibited an appreciable CT absorption over 500 nm (Supplementary Fig. 1). This power-law emission decay indicates the generation of intermediate charge-separated states and successive gradual bulk charge recombination, which led to LPL. The emission spectra of these films were attributed to the CT excited states between the donors and acceptors[16,17].

The TPP$^+$/TPBi, TPP$^+$/*m*CBP and MeOTPP$^+$/*m*CBP films form ^{1}CT excited states (Fig. 2b) and the ^{1}CT energy levels are lower than those of the locally excited states of donors and acceptors (^3LE_D and ^3LE_A). Therefore, the LPL that was caused by the recombination of accumulated charges occurs from the CT states. Because the Φ_{PL} of the CT excited states is low, the non-radiative deactivation pathway from the CT excited state to the ground state is also available. The TPP$^+$/TPBi film exhibits a CT emission at 603 nm with a shoulder peak at ~555 nm. The shoulder peak decreased with an increase in TPP$^+$ concentration because of the self-absorption of TPP radicals at 500–600 nm (Supplementary Fig. 5a)[17,40,41] and disappeared at the higher TPP$^+$ concentration due to the strong self-absorption of the TPP radical (Supplementary Fig. 5b). The TPP$^+$/TPBi film showed the longest LPL duration of 1,830 s. The LPL duration decreased with an increase in TPP$^+$ concentration because the charge recombination probability increased at the higher TPP$^+$ concentration (Supplementary Fig. 5c).

The TPP$^+$/*m*CBP film exhibited a broad NIR emission at 731 nm from the smaller energy gap between the TPP$^+$ LUMO and *m*CBP HOMO. Because of the low Φ_{PL} of the CT emission and low NIR sensitivity of the photodiode for detection, the LPL duration was 33 s. The MeOTPP$^+$/*m*CBP films exhibited a CT emission at 624 nm with an LPL

duration of 610 s. In contrast, the $MeOTPP^+$/TPBi film did not form a CT excited state although the HOMO and LUMO levels were appropriate. The TPBi may not act as a donor because of the closed HOMO levels between them. Instead, this film exhibited the fluorescence and RTP of the $MeOTPP^+$ (Supplementary Fig. 6). These results indicate that the formation of the lowest ^{1}CT state is important for efficient LPL emission in p-type OLPL systems.

As a blended film of donor and acceptor molecules has donor, acceptor and charge-transfer absorption bands, OLPL systems can be excited by various wavelengths, offering a major advantage over inorganic LPL systems, which are limited mostly to ultraviolet to blue excitation wavelengths. The excitation spectra of the TPP^+/TPBi and $MeOTPP^+$/*m*CBP films indicate that these films can be excited by wavelengths from 300 to 600 nm (Supplementary Fig. 7). To confirm the excitation wavelength dependence of the LPL emission, these films were excited by 365, 400, 455, 500, 550 and 600 nm light-emitting diodes (LEDs). The LPL emission was observed at all excitation wavelengths, although the LPL duration decreased, which correlates with the absorption intensity (Supplementary Figs. 2c and 6c). Unlike the emission lifetime from normal excited states, such as conventional fluorescence and phosphorescence, the duration of the LPL depends on the number of stored charges and varies with the excitation wavelength. When the hot exciton mechanism is considered as the charge separation process, the charge separation efficiency also depends on the excitation wavelength[42,43]. The 600 nm photoexcitation and NIR LPL emission, which corresponds to the biological window, is expected to be suitable for bioimaging[44].

The LPL performance improved sevenfold with addition of hole-trapping material to the p-type OLPL system. Previously, we reported that the LPL duration could be enhanced

by doping electron-trapping materials into an n-type OLPL system[13]. The dopants can receive electrons from the acceptor molecules because the LUMO of the dopant is lower than that of the acceptor. By tuning the appropriate LUMO level, the trapped electrons remained for more than one week[45]. In the p-type OLPL system, TCTA was doped into the TPP^+/TPBi system as the HOMO level of the TCTA (−5.3 eV) was shallower than that of the TPBi (−6.0 eV) (Fig. 1d and Supplementary Fig. 2). The PL and LPL spectra of the TPP^+/TPBi/TCTA film with a 1:99:1 molar ratio (Fig. 3a) was nearly identical to that of the TPP^+/TPBi film (Fig. 2b), except that the LPL duration time was significantly improved almost sevenfold, to 14,600 s (Fig. 3b). The TPBi/TCTA (99:1) film also exhibited no LPL because of the closed LUMO levels between them, although it formed a CT excited state (Supplementary Fig. 8). This result indicates that the TCTA can act as a hole trap (Fig. 3c).

To confirm the hole trapping by TCTA, the absorption spectra of TPP^+/TPBi, TPP^+/TPBi/TCTA and TPBi/TCTA films were obtained[45]. After photoexcitation, a clear broad absorption above 800 nm was observed in the TPP^+/TPBi/TCTA film (Fig. 3d). This peak corresponds to the radical cation of TCTA in dichloromethane (DCM) under electrochemical oxidation, although a wavelength shift can be observed because of the polarization effect in the solid film (Fig. 3d). In contrast, the TPBi/TCTA film exhibited no absorption of the TCTA radical cation after photoexcitation (Fig. 3d). Therefore, the formation of the TCTA radical cations in the TPP^+/TPBi/TCTA film indicates a hole diffusion from a TPBi radical cation to a TCTA molecule. The hole trapping was confirmed by the temperature dependence of the LPL duration[46]. Because hole detrapping is endothermic, the LPL intensity increased by raising the temperature in the TPP^+/TPBi/TCTA film (Supplementary Fig. 9b). In contrast, the LPL duration of the

193 TPP^+/TPBi film decreased gradually with an increase in temperature because the non-
194 radiative process was enhanced at high temperatures (Supplementary Fig. 9c). Thus,
195 detrapping in the TPP^+/TPBi/TCTA film for the LPL intensity overwhelmed the non-
196 radiative process at the measured temperatures.

197 To confirm the generality of the hole-trapping mechanism, several trap molecules
198 with different HOMO levels (PPT, *m*CBP and α-NPD) were investigated (Supplementary
199 Fig. 10). While the LPL emission spectra were the same for all systems, the emission
200 duration varied significantly. These differences mainly depend on the HOMO levels,
201 suggesting the LPL emission originates from the hole diffusion mechanism. Since the
202 HOMOs of PPT (−5.9 eV) and *m*CBP (−5.7 eV) are comparable to that of TPBi (−6.0 eV),
203 they do not act as effective traps because the holes can easily detrap at room temperature.
204 However, the HOMOs of both TCTA (−5.3 eV) and α-NPD (−5.2 eV) are located at much
205 shallower levels compared with that of TPBi, and therefore provide effective hole traps.
206 The generation of α-NPD radical cation was also confirmed by excited-state absorption
207 spectra (Supplementary Fig. 10e). These results suggest the large HOMO gap (<0.5 eV)
208 is required for efferent hole traps at room temperature.

209 Optical analysis of TPP^+/TPBi, $MeOTPP^+$/*m*CBP and TPP^+/TPBi/TCTA films was
210 carried out in air to confirm the LPL emission of the p-type OLPL systems because the
211 LUMO levels of the TPP^+ (−4.0 eV) and $MeOTPP^+$ (−3.8 eV) are lower than the reduction
212 potential of oxygen (−3.5 eV). Although the reported n-type OLPL system of *m*-
213 MTDATA/PPT showed no LPL emission in air (Supplementary Fig. 9a), all p-type OLPL
214 films exhibited LPL in air (Fig. 4a,b and Supplementary Fig. 11b). However, the observed
215 LPL durations of all films in air were shorter than in nitrogen because the energy transfer
216 from the triplet excited state of the emitters to the molecular oxygen with a triplet ground

state (triplet quenching) cannot be prevented[47]. An irreversible reaction between TPP radical and oxygen is known[48]; however, this reaction is considered to be slow in the solid state because the LPL intensity recovers considerably with evacuation (Supplementary Fig. 12). On the other hand, because of the irreversible reaction with oxygen, the emission intensity does not recover completely. The charge recombination in LPL emission generates ^{1}CT and ^{3}CT excited states[49], and the ^{3}CT excited states are quenched by oxygen. In contrast, the emission spectra did not change because of the lack of ^{3}LE contribution (Fig. 4c,d). In addition to oxygen, water also can deactivate the radicals. To confirm the LPL quenching by water, the crushed TPP^{+}/TPBi/TCTA sample was dispersed into water and excited at 365 nm (Supplementary Fig. 13 and Supplementary Video 1). As a result, LPL was also observed in water. Due to the slow diffusion of water into the solid samples, the effect of quenching by water is very small.

The LPL duration of the TPP^{+}/TPBi/TCTA in air was extended to 1,685 s, which is almost the same as the TPP^{+}/TPBi film in nitrogen (Supplementary Video 2).

These results indicate that the p-type OLPL system with deep HOMO levels can emit LPL in air but cannot prevent triplet quenching by oxygen. Future developments of low-oxygen-diffusion hosts or advanced encapsulation techniques to prevent oxygen are required to obtain efficient LPL emissions in air.

We demonstrated p-type OLPL systems based on the cationic organic photoredox catalyst TPP^{+} and $MeOTPP^{+}$ as acceptors. These systems can be excited by a wavelength from the ultraviolet range to 600 nm and exhibit a yellow-to-NIR LPL emission. The p-type OLPL with deeper HOMO and LUMO levels can prevent reaction with oxygen and exhibited LPL in air. The hole-trapping dopant enhanced the LPL duration strongly without changing the emission spectrum. The tunable absorption wavelength from 300 to

600 nm of OLPL systems provides a major advantage over inorganic materials, and the absorptions and emissions that were fitted to the biological window are expected to have future bioimaging applications. For efficient charge separation, the oxidized state of the donor and the reduced state of the acceptor must be stable. For the hole-trapping mechanism, the electron donor, acceptor and trap molecules need to have a cascading HOMO and LUMO relationship. The hole-trapping material requires an energy gap of about 0.5 eV shallower than the acceptor's HOMO level for efficient hole trapping. For efficient LPL emission, the CT excited state needs to be lower than that of the ^{3}LE. For the melt-cast process, the donor host needs to form good amorphous films. The p-type OLPLs can prevent reaction with oxygen in the excited state, making it possible to produce LPL films by a simple solution processing. However, because triplet quenching by oxygen cannot be prevented perfectly in amorphous films, low-oxygen-diffusion hosts or oxygen barrier materials are required for future practical applications. Future development of p-type OLPL made by polymers will enable printable and flexible film OLPL systems.

Acknowledgements

This work was supported by the Japan Science and Technology Agency (JST) FOREST project (grant number JPMJFR201H); JST ERATO, Adachi Molecular Exciton Engineering Project (grant number JPMJER1305); JSPS KAKENHI (grant numbers JP18H02049 and JP21H02020); JSPS Core-to-core project; the International Institute for Carbon Neutral Energy Research (WPI-I2CNER) sponsored by the Ministry of Education, Culture, Sports, Science, and Technology (MEXT), the OIST Proof of Concept (POC)

Programme; and the Kyushu University Platform of Inter/Transdisciplinary Energy Research, young researcher/doctor student support programme. We thank K. Tokumaru for helpful discussions. We thank K. Kusuhara and N. Nakamura for their assistance with the preparation of TPBi, *m*CBP and TCTA.

Author contributions

K.J. and R.K. designed this project. K.J. and R.K. carried out all the experiments. K.J and Z.L. performed the electrochemical and in situ spectroelectrochemical measurements. K.J. and R.K. analysed all data. R.K and C.A. supervised the project. All authors contributed to writing the paper and critically commented on the project.

Competing interests

The authors declare no competing interests.

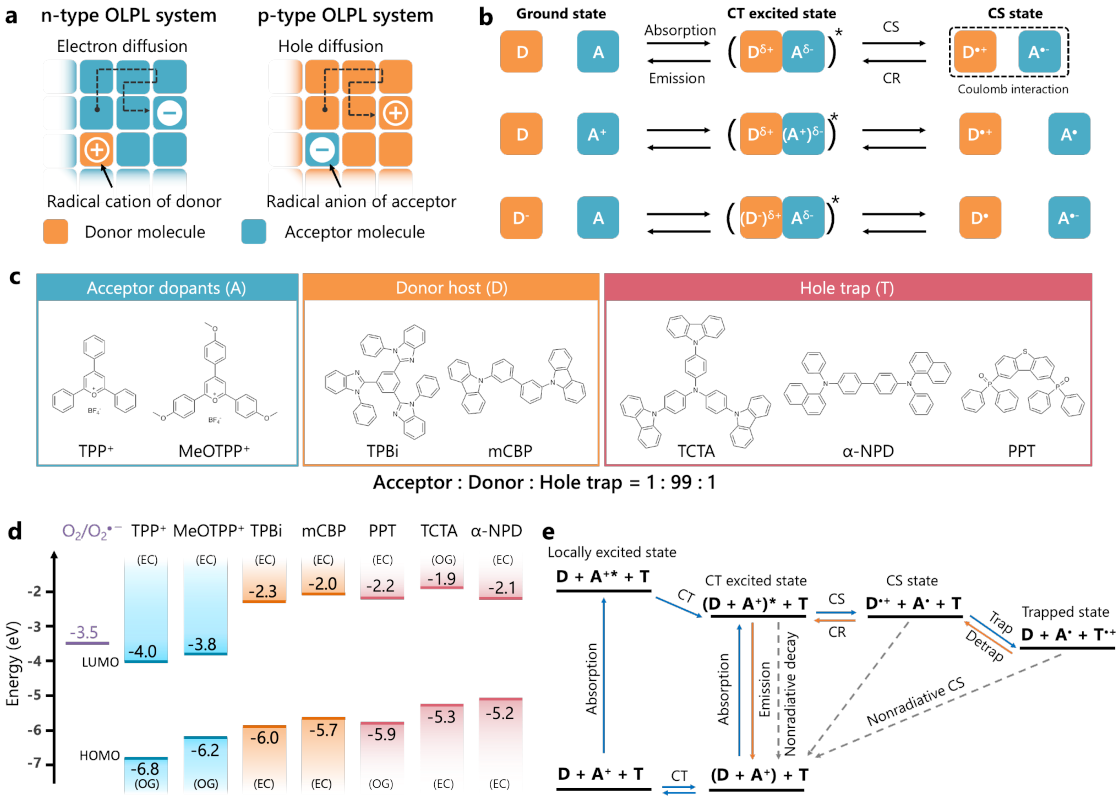

Figure 1. Emission mechanism of p-type OLPL system. (**a**) Schematic diagrams showing charge-separated states in n-type (left) and p-type (right) OLPL systems. In n-type systems, electrons diffuse through the host acceptor molecules until they recombine radiatively with a radical donor cation. In p-type systems, hole diffusion occurs in a donor host until charges recombine with a radical acceptor anion. (**b**) A mixture of neutral donors and acceptors forms radical ion pair with Coulomb interaction as the charge-separated (CS) state by photo-induced charge-transfer (CT) from the ground state, whereas cationic acceptors or anionic donors form neutral radicals. The weaker Coulomb interaction is expected to reduce the charge recombination (CR) probability. (**c**) Chemical structures of electron acceptors, donors, and hole-trap molecules. (**d**) Highest occupied molecular orbital (HOMO) and lowest unoccupied molecular orbital (LUMO) levels of materials and reduction potential of oxygen. HOMO and LUMO levels were obtained

from electrochemical (EC) measurements. When the redox potential was out of the range of electrochemical measurement, the HOMO and LUMO levels were estimated from the optical gap (OG) that was calculated from the absorption edge. (**e**) Schematic diagram of p-type OLPL having hole-trap mechanism.

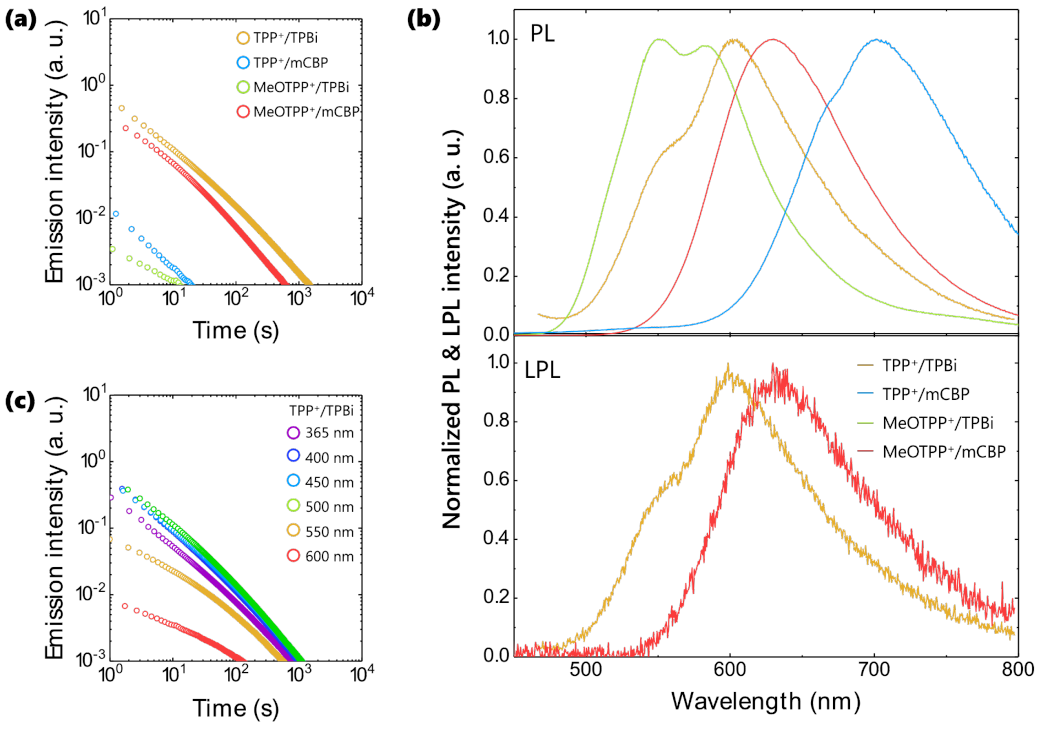

Figure 2. Photoluminescence properties of OLPL systems under nitrogen gas. (a) Emission decay profiles (excitation: 365 nm, 1 mW, 300 s, 300 K, under N_2) of TPP^+/TPBi, TPP^+/*m*CBP, $MeOTPP^+$/TPBi, and $MeOTPP^+$/*m*CBP films in log-log plot. **(b)** Steady-state photoluminescence (PL) spectra and emission spectra 10 s after photoexcitation (LPL) (excitation: 365 nm, 1 mW, 300 s, 300 K, under N_2). The LPL spectrum of the TPP^+/*m*CBP was not measurable because of the weak emission intensity excited at 365 nm. **(c)** Excitation-wavelength dependence of emission decay profiles of TPP^+/TPBi film (excitation: 300 mW, 300 s, 300 K, under N_2).

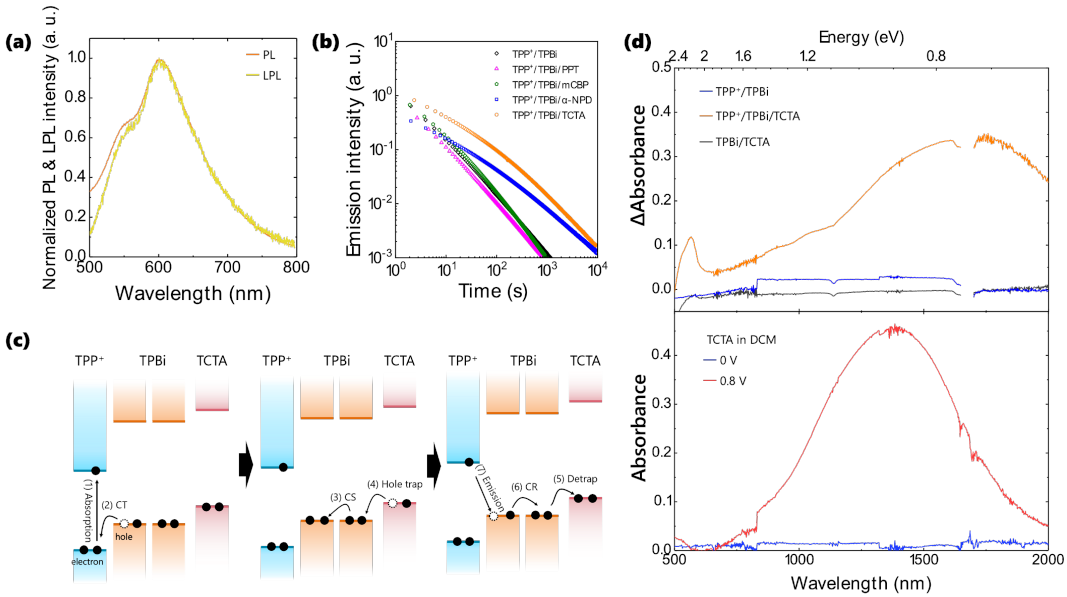

Figure 3. Photoluminescence properties of TPP^+/TPBi/TCTA film under nitrogen gas. (a) PL and LPL (delay = 10 s) spectra of TPP^+/TPBi/TCTA film (excitation: 365 nm, 1 mW, 300 s, 300 K, under N_2). **(b)** Emission decay profiles (excitation: 365 nm, 1 mW, 300 s, 300 K, under N_2) of TPP^+/TPBi, TPP^+/TPBi/PPT, TPP^+/TPBi/mCBP, TPP^+/TPBi/TCTA, and TPP^+/TPBi/α-NPD films. **(c)** Emission mechanism of TPP^+/TPBi/TCTA film. The TCTA molecule accepts holes from TPBi and forms radical cations as the HOMO level of the TCTA is shallower than that of the TPBi. Thermal detrapping from TCTA regenerates radical cations of TPBi and recombines with TPP radical. **(d)** (Top) Delta absorption spectra of TPP^+/TPBi, TPP^+/TPBi/TCTA, and TPBi/TCTA films before and after photoexcitation (300 K, under N_2). (Bottom) Absorption spectra of TCTA in DCM that contains 0.1 M $TBAPF_6$ with and without electrical oxidation (300 K, under N_2). Absorption data at 1650-1700-nm was omitted because of the quartz substrate absorption.

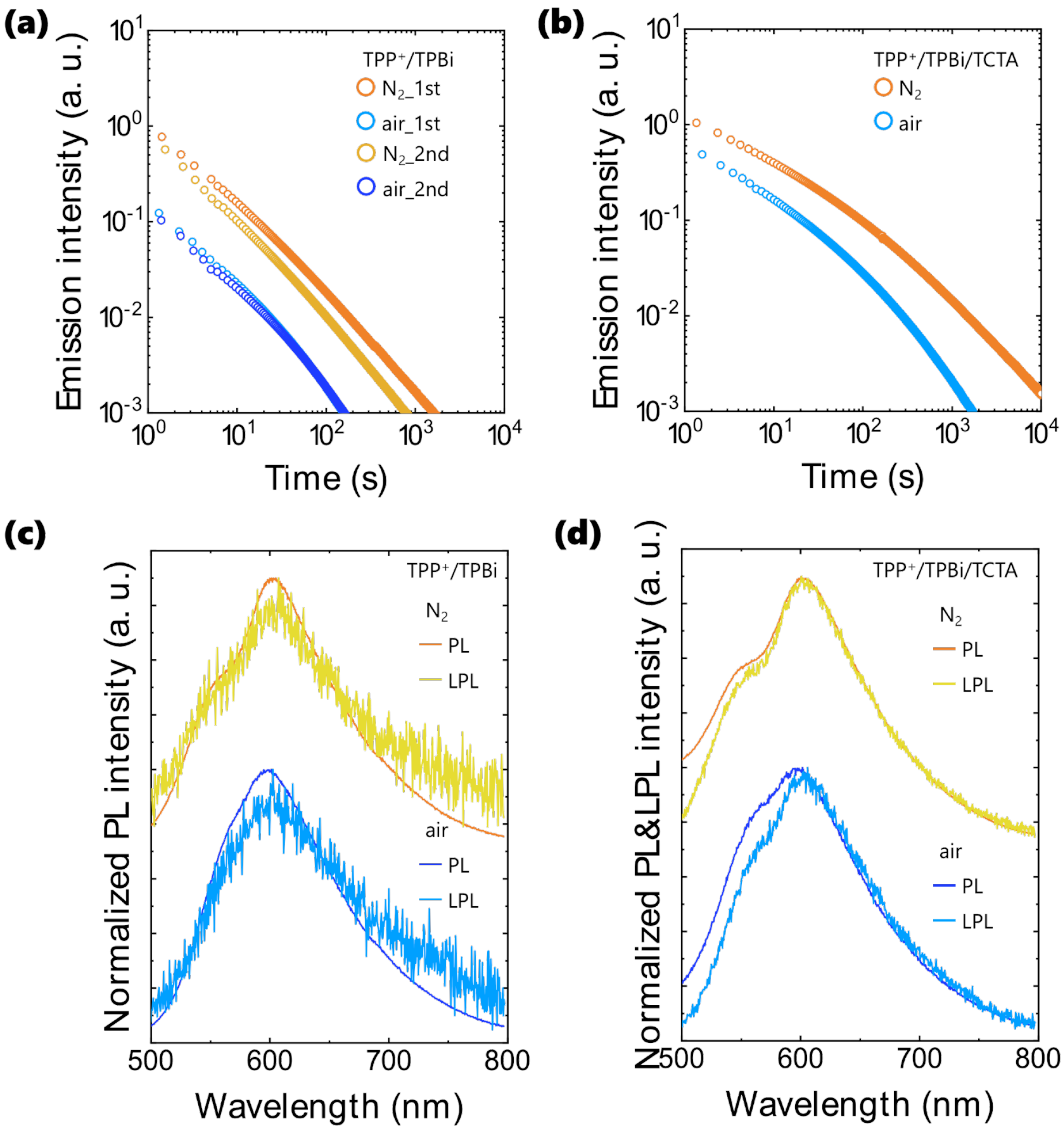

Figure 4. Optical properties of OLPL systems in air. LPL duration under N_2 and in air of TPP^+/TPBi (a) and TPP^+/TPBi/TCTA (b) films excited at 365 nm. The optical properties were obtained under N_2, and then after exposure to air for 24 hours. The sample was evacuated again, and the second measurements were repeated. PL and LPL (delay = 10 s) spectra in vacuum and in air of TPP^+/TPBi (c) and TPP^+/TPBi/TCTA (d) films excited at 365 nm.

References

1. Xu, J. & Tanabe, S. Persistent luminescence instead of phosphorescence: History, mechanism, and perspective. *J. Lumin.* **205**, 581–620 (2019).

2. Li, Y., Gecevicius, M. & Qiu, J. Long persistent phosphors—from fundamentals to applications. *Chem. Soc. Rev.* **45**, 2090–2136 (2016).

3. Ueda, J., Miyano, S. & Tanabe, S. Formation of Deep Electron Traps by Yb^{3+} Codoping Leads to Super-Long Persistent Luminescence in Ce^{3+} -Doped Yttrium Aluminum Gallium Garnet Phosphors. *ACS Appl. Mater. Interfaces* **10**, 20652–20660 (2018).

4. Majewska, N. *et al.* Study of persistent luminescence and thermoluminescence in $SrSi_2N_2O_2:Eu^{2+},M^{3+}$ (M = Ce, Dy, and Nd). *Phys. Chem. Chem. Phys.* **22**, 17152–17159 (2020).

5. Vitola, V., Millers, D., Bite, I., Smits, K. & Spustaka, A. Recent progress in understanding the persistent luminescence in $SrAl_2O_4$:Eu,Dy. *Mater. Sci. Technol.* **35**, 1661–1677 (2019).

6. Dorenbos, P. Mechanism of persistent luminescence in $Sr_2MgSi_2O_7:Eu^{2+}$; Dy^{3+}. *Phys. status solidi* **242**, R7–R9 (2005).

7. Li, Y. *et al.* Long persistent and photo-stimulated luminescence in Cr^{3+}-doped Zn–Ga–Sn–O phosphors for deep and reproducible tissue imaging. *J. Mater. Chem. C* **2**, 2657 (2014).

8. Zhuang, Y., Ueda, J., Tanabe, S. & Dorenbos, P. Band-gap variation and a self-redox effect induced by compositional deviation in $ZnxGa_2O_{3+x}:Cr^{3+}$ persistent phosphors. *J. Mater. Chem. C* **2**, 5502 (2014).

9. Wu, S., Pan, Z., Chen, R. & Liu, X. *Long Afterglow Phosphorescent Materials* (Springer 2017).

10. Kabe, R. & Adachi, C. Organic long persistent luminescence. *Nature* **550**, 384–387 (2017).

11. Jinnai, K., Nishimura, N., Kabe, R. & Adachi, C. Fabrication-method Independence of Organic Long-persistent Luminescence Performance. *Chem. Lett.* **48**, 270–273 (2019).

12. Lin, Z., Kabe, R., Nishimura, N., Jinnai, K. & Adachi, C. Organic Long-Persistent Luminescence from a Flexible and Transparent Doped Polymer. *Adv. Mater.* **30**, 1803713 (2018).

13. Jinnai, K., Kabe, R. & Adachi, C. Wide-Range Tuning and Enhancement of Organic Long-Persistent Luminescence Using Emitter Dopants. *Adv. Mater.* **30**, (2018).

14. Hirata, S. Recent Advances in Materials with Room-Temperature Phosphorescence: Photophysics for Triplet Exciton Stabilization. *Adv. Opt. Mater.* **5**, 1700116 (2017).

15. Notsuka, N., Kabe, R., Goushi, K. & Adachi, C. Confinement of Long-Lived Triplet Excitons in Organic Semiconducting Host-Guest Systems. *Adv. Funct. Mater.* **27**, 1703902 (2017).

16. Nishimura, N., Lin, Z., Jinnai, K., Kabe, R. & Adachi, C. Many Exciplex Systems Exhibit Organic Long-Persistent Luminescence. *Adv. Funct. Mater.* **30**, 2000795 (2020).

17. Lin, Z., Kabe, R., Wang, K. & Adachi, C. Influence of energy gap between charge-transfer and locally excited states on organic long persistence luminescence. *Nat. Commun.* **11**, 191 (2020).

18. Bhattacharjee, I. & Hirata, S. Highly Efficient Persistent Room-Temperature

Phosphorescence from Heavy Atom-Free Molecules Triggered by Hidden Long Phosphorescent Antenna. *Adv. Mater.* **32**, 2001348 (2020).

19. Alam, P. *et al.* Two Are Better Than One: A Design Principle for Ultralong-Persistent Luminescence of Pure Organics. *Adv. Mater.* **32**, 2001026 (2020).

20. Usta, H. *et al.* Design, synthesis, and characterization of ladder-type molecules and polymers. air-stable, solution-processable n-channel and ambipolar semiconductors for thin-film transistors via experiment and theory. *J. Am. Chem. Soc.* **131**, 5586–5608 (2009).

21. de Leeuw, D. M., Simenon, M. M. J., Brown, A. R. & Einerhand, R. E. F. Stability of n-type doped conducting polymers and consequences for polymeric microelectronic devices. *Synth. Met.* **87**, 53–59 (1997).

22. Zhou, K., Dong, H., Zhang, H. & Hu, W. High performance n-type and ambipolar small organic semiconductors for organic thin film transistors. *Phys. Chem. Chem. Phys.* **16**, 22448–22457 (2014).

23. Romero, N. A. & Nicewicz, D. A. Organic Photoredox Catalysis. *Chem. Rev.* **116**, 10075–10166 (2016).

24. Fukuzumi, S. *et al.* Electron-transfer state of 9-mesityl-10-methylacridinium ion with a much longer lifetime and higher energy than that of the natural photosynthetic reaction center. *J. Am. Chem. Soc.* **126**, 1600–1601 (2004).

25. Todd, W. P., Dinnocenzo, J. P., Farid, S., Goodman, J. L. & Gould, I. R. Efficient photoinduced generation of radical cations in solvents of medium and low polarity. *J. Am. Chem. Soc.* **113**, 3601–3602 (1991).

26. Jia, D. Charging curves and excitation spectrum of long persistent phosphor $SrAl_2O_4:Eu^{2+}$, Dy^{3+}. *Opt. Mater. (Amst).* **22**, 65–69 (2003).

27. Jia, D., Zhu, J. & Wu, B. Correction of excitation spectra of long persistent phosphors. *J. Lumin.* **90**, 33–37 (2000).

28. Wintgens, V., Pouliquen, J., Kossanyi, J., Williams, J. L. R. & Doty, J. C. Emission of substituted pyrylium and thiapyrylium salts: Phosphorescence and delayed fluorescence emission in polymeric matrices. *Polym. Photochem.* **6**, 1–20 (1985).

29. Farid, S., Dinnocenzo, J. P., Merkel, P. B., Young, R. H. & Shukla, D. Bimolecular Electron Transfers That Follow a Sandros−Boltzmann Dependence on Free Energy. *J. Am. Chem. Soc.* **133**, 4791–4801 (2011).

30. Perkowski, A. J., You, W. & Nicewicz, D. A. Visible Light Photoinitiated Metal-Free Living Cationic Polymerization of 4-Methoxystyrene. *J. Am. Chem. Soc.* **137**, 7580–7583 (2015).

31. Schrögel, P. *et al.* Meta-linked CBP-derivatives as host materials for a blue iridium carbene complex. *Org. Electron.* **12**, 2047–2055 (2011).

32. Jiang, Z.-L., Tian, W., Kou, Z.-Q., Cheng, S. & Li, Y.-H. The influence of the mixed host emitting layer based on the TCTA and TPBi in blue phosphorescent OLED. *Opt. Commun.* **372**, 49–52 (2016).

33. Kuwabara, Y., Ogawa, H., Inada, H., Noma, N. & Shirota, Y. Thermally stable multilared organic electroluminescent devices using novel starburst molecules, 4,4′,4″-Tri(N-carbazolyl)triphenylamine (TCTA) and 4,4′,4″-Tris(3-methylphenylphenylamino)triphenylamine (*m*-MTDATA), as hole-transport materials. *Adv. Mater.* **6**, 677–679 (1994).

34. Jinnai, K., Nishimura, N., Adachi, C. & Kabe, R. Thermally activated processes in an organic long-persistent luminescence system. *Nanoscale* **13**, 8412–8417 (2021).

35. Goushi, K., Yoshida, K., Sato, K. & Adachi, C. Organic light-emitting diodes

employing efficient reverse intersystem crossing for triplet-to-singlet state conversion. *Nat. Photonics* **6**, 253–258 (2012).

36. Hamill, W. H. Debye–Edwards electron recombination kinetics. *J. Chem. Phys.* **71**, 140–142 (1979).

37. Tachiya, M. & Seki, K. Unified explanation of the fluorescence decay and blinking characteristics of semiconductor nanocrystals. *Appl. Phys. Lett.* **94**, 081104 (2009).

38. Niizuma, S. *et al.* Free Radicals Produced from the Derivatives of Pyrylium Salts in Solution by Photoillumination. *Bull. Chem. Soc. Jpn.* **58**, 2600–2607 (1985).

39. Miranda, M. A. & García, H. 2,4,6-Triphenylpyrylium Tetrafluoroborate as an Electron-Transfer Photosensitizer. *Chem. Rev.* **94**, 1063–1089 (1994).

40. Grancini, G. *et al.* Hot exciton dissociation in polymer solar cells. *Nat. Mater.* **12**, 29–33 (2013).

41. Gelinas, S. *et al.* Ultrafast Long-Range Charge Separation in Organic Semiconductor Photovoltaic Diodes. *Science.* **343**, 512–516 (2014).

42. Lochner, C. M., Khan, Y., Pierre, A. & Arias, A. C. All-organic optoelectronic sensor for pulse oximetry. *Nat. Commun.* **5**, 5745 (2014).

441 43. Sakurai, M. *et al.* Organic photostimulated luminescence associated with
442 persistent spin-correlated radical pairs. Commun. Mater. 2, 74 (2021).
443 44. Ueda, J., Harada, M., Miyano, S., Yamada, A. & Tanabe, S. Pressure-induced
444 variation of persistent luminescence characteristics in $Y_3Al_{5-x}Ga_xO_{12}:Ce^{3+}$–$M^{3+}$
445 (M = Yb, and Cr) phosphors: opposite trend of trap depth for 4f and 3d metal ions.
446 *Phys. Chem. Chem. Phys.* **22**, 19502–19511 (2020).
447 45. Hasebe, N. *et al.* Absolute Phosphorescence Quantum Yields of Singlet Molecular
448 Oxygen in Solution Determined Using an Integrating Sphere Instrument. *Anal.*
449 *Chem.* **87**, 2360–2366 (2015).
450 46. Akaba, R., Sakuragi, H. & Tokumaru, K. Triphenylpyrylium-salt-sensitized
451 electron transfer oxygenation of adamantylideneadamantane. Product,
452 fluorescence quenching, and laser flash photolysis studies. *J. Chem. Soc. Perkin*
453 *Trans. 2* **1**, 291 (1991).
454 47. Baldo, M. A., O'Brien, D. F., Thompson, M. E. & Forrest, S. R. Excitonic singlet-
455 triplet ratio in a semiconducting organic thin film. *Phys. Rev. B* **60**, 14422–14428
456 (1999).

48. Fan, C. *et al.* Dibenzothiophene-Based Phosphine Oxide Host and Electron-Transporting Materials for Efficient Blue Thermally Activated Delayed Fluorescence Diodes through Compatibility Optimization. *Chem. Mater.* **27**, 5131–5140 (2015).

49. Liu, Y., Liu, M. S. & Jen, A. K.-Y. Synthesis and characterization of a novel and highly efficient light-emitting polymer. *Acta Polym.* **50**, 105–108 (1999).

Data availability

The datasets for Figs. 2–4 are available in the source data section. Additional information is available from the authors on request.

Methods

Materials: TPP^+, $MeOTPP^+$, and *m*-MTDATA were from MERCK (Darmstadt, Germany). TPBi, *m*CBP, and α-NPD were from TCI Chemical (Tokyo, Japan). PPT was synthesized according to literature[48].

Film fabrication: In a nitrogen-filled glovebox, mixtures of electron donors and acceptors were placed on a template glass substrate with a 100-mm^2 surface area, 0.5-mm depth, and heated to 280 °C for 10 s. After melting, the substrate was cooled rapidly to room temperature.

Optical and electrical measurements: A dichloromethane solution of each material (10^{-5} M) was used to measure absorption, fluorescence, phosphorescence, and absolute photoluminescence quantum yields (Φ_{PL}). The absorption spectra were measured using a UV–vis–NIR spectrophotometer (LAMBDA 950, Perkin Elmer). The photoluminescence spectra at room temperature and the phosphorescence spectra at 77 K were measured using spectrofluorometers (FP-8600, JASCO, and PMA-12, Hamamatsu Photonics). The Φ_{PL} were measured using an integrating sphere with a photoluminescence measurement unit (Quantaurus-QY, C11347-01, Hamamatsu Photonics) in a glovebox. Sample was excited by 365-nm LED (0.1 mW) for 60 s. Emission spectra were obtained each 20 ms integration time during photoexcitation (60 s) and after photoexcitation (60 s). Photoluminescence lifetime was measured using a streak camera system (C14832-110, Hamamatsu Photonics). Samples were photoexcited by 343-nm femtosecond (pulse

488 width 190 fs, 1 kHz) laser (Pharos and HERO, Light Conversion). The phosphorescence
489 lifetime of TPP^+ and $MeOTPP^+$ was obtained by time-resolved emission spectra at 77 K
490 measured by spectrometers (PMA-12, Hamamatsu Photonics). Cyclic voltammetry and
491 differential pulse voltammetry were carried out using an electrochemical analyser (Model
492 610, BAS). Measurements were performed in dried and oxygen-free DMF or THF using
493 0.1 M tetrabutylammonium hexafluorophosphate as a supporting electrolyte. A platinum
494 wire was used as a counter electrode, with glassy carbon as a working electrode, and
495 Ag/Ag^+ as a reference electrode. Redox potentials were referenced against
496 ferrocene/ferrocenium (Fc/Fc^+). Corresponding HOMO and LUMO energies were
497 calculated from first reduction or oxidation peaks using an absolute value of –4.8 eV to
498 vacuum for the Fc/Fc^+ redox potential[49]. The absorption spectra of the TPP^+, TCTA and
499 α-NPD radical species were measured by the *in situ* UV–vis–NIR spectroelectrochemical
500 technique. The UV-vis-NIR spectrophotometer is UV-3600 Plus, SHIMADZU. TPP^+,
501 TCTA, and α-NPD radical cations were generated by electrical oxidation on the platinum
502 mesh electrode surface in a DCM solution that contained 0.1 M $TBAPF_6$ (BAE, 013510
503 SEC-C, Thin layer quartz glass spectroelectrochemical cell kit) using an electrochemical
504 analyzer (BAS, Model 610E). The absorption spectra of TCTA and α-NPD radical cations
505 were obtained 30 s after photoexcitation by a 365-nm LED light. X-ray diffraction (XRD)
506 analysis was performed by Bruker, D8 Discover.

507 **LPL measurements:** The LPL spectra and decay profiles were obtained using a
508 measurement system in a glovebox[13]. The fabricated films were placed in a dark box and
509 excited by various LEDs wavelengths with bandpass filters (Thorlabs, band width ± 5
510 nm), an excitation power of 1 $mWcm^{-2}$, and an excitation duration of 300 s. The PL and
511 LPL spectra were recorded using a multichannel spectrometer (PMA-12, Hamamatsu

Photonics). Emission decay profiles were obtained without wavelength sensitivity calibration using a silicon photomultiplier (MPPC module, C13366-1350GA, Hamamatsu Photonics). The temperature dependence and air stability were measured in a cryostat (PS-HT-200, Nagase Techno-Engineering) connected to a turbo molecular pump (HiPace, Pfeiffer Vacuum) and excited for 60 s. The LPL properties were measured under a vacuum. Samples were kept under air (humidity: 30-40%) in the dark for one week and the optical properties were measured in air.